JOURNAL OF MATERIALS SCIENCE 31 (1996) 2353–2360

Effect of composition on the physicochemical properties of nickel aluminium hydrotalcites

S. KANNAN, A. NARAYANAN, C. S. SWAMY
Department of Chemistry, Indian Institute of Technology, Madras 600 036, India

Ni–Al hydrotalcite compounds with the structural formula $[Ni_{1-x}Al_x(OH)_2]^{x+}$ $[(CO_3)_{x/2} \cdot mH_2O]^{x-}$ were synthesized in the composition range Al/Ni+Al (x) = 0.20–0.50 by sequential precipitation. The samples were characterized by X-ray diffraction, infrared absorption, thermogravimetry–differential scanning calorimetry–evolved gas analysis, transmission electron microscopy and BET surface-area measurements. The crystallinity and the lattice parameters of the samples are significantly affected with respect to composition. Hydrothermal treatments performed on the aged samples enhanced the crystallinity. The nitrate ion is also present along with carbonate ion as the charge-balancing anion in the interlayer space. The thermal stability of these materials increased with decrease in Ni/Al atomic ratio. Thermal calcination of these compounds yielded non-stoichiometric NiO whose crystallinity and thermal stability depends on the composition as well as on calcination temperature.

1. Introduction

Hydrotalcite-like materials (HT-like) are a new class of materials, which have received considerable attention in the last two decades owing to their potential applications as anion exchangers, adsorbents and, most importantly, as precursors for the synthesis of multicomponent catalysts [1–7]. These materials possess positively charged layers of bi- and trivalent metal hydroxides interspersed with anion and water molecules in the interlayer positions. The basic structure of these materials stems from brucite, $Mg(OH)_2$, in which the bivalent ion occupies the octahedral position (surrounded by six OH groups), forming infinite sheets through edge sharing held by hydrogen bonding. When the bivalent cation is substituted by a trivalent ion, a positive charge density is created in the layer. Anions and water molecules occupy the interlayer position in order to maintain the electrical neutrality. They are represented by the general formula $[M(II)_{1-x}M(III)_x(OH)_2]^{x+}[A^{n-}_{x/n}]^{x-} \cdot mH_2O$ where M(II) and M(III) are bi- and trivalent cations, A is the interlayer anion and x can have values between 0.15 and 0.40.

The M(II)/M(III) composition plays a pivotal role in controlling the structure and properties of these materials [8, 9]. The purpose of the present investigation was to study the influence of Ni/Al atomic ratio on the structure and physicochemical properties of Ni–Al HT-like compounds.

2. Experimental procedure

2.1. Sample preparation

The samples were prepared by a sequential precipitation method wherein the precipitants, namely $NaOH/Na_2CO_3$ mixture (0.2 mol/0.015 mol) dissolved in 50 ml of water, are added to nickel nitrate and aluminium nitrate solutions of appropriate concentrations with increasing pH under stirring. The addition took nearly 1 h and the final pH was kept at 10. The slurry obtained was aged at 65 °C for 24 h, filtered, washed thoroughly with distilled water (until neutral) and dried in an air oven at 80 °C overnight. Hydrothermal treatment was performed on a portion of the aged sample in a Teflon coated autoclave at 110 °C for 2 days under autogenous conditions.

2.2. Measurements

Elemental analysis of Ni^{2+} and Al^{3+} were carried out by inductively coupled plasma emission spectrometry (ICPES, Model 3410, ARL) by dissolving the samples in a minimum amount of dilute hydrochloric acid. The powder X-ray diffraction patterns were recorded in a Philips X-ray generator (Model PW 1050/81 controlled by PW 1710 unit) using nickel-filtered CuK_α radiation ($\lambda = 0.154\,16$ nm) with silicon as external standard. Infrared absorption spectra were recorded using Perkin–Elmer Fourier transform–infrared (FT–IR) spectrometer (Model 1760) in the form of KBr discs. Thermogravimetric–differential scanning calorimetry (TG–DSC) studies were carried out in a Perkin–Elmer TGA–DSC/7 at a heating rate of 10 °C min^{-1} under a nitrogen atmosphere. Transmission electron micrographs were taken in a Philips transmission electron microscope (Model CM12, Holland, $h\nu = 120$ kV) by keeping the sample in a carbon-coated copper grid. The BET (N_2) surface area of the samples were measured in a Carlo Erba (Model 1800) sorptometer at 77 K. Hereafter, the samples are

0022–2461

TABLE I Chemical composition, lattice parameters and surface area of the samples synthesized

Compound	Ni/Al atomic ratio		a (nm)	c (nm)	V (10^{-3} nm^3)	Surface area ($m^2\ g^{-1}$)
	Calc.	Meas.				
NiAl2.0:1-A	2.0	2.1	0.3020	2.2432	177.2	92
NiAl2.5:1-A	2.5	2.6	0.3029	2.2444	178.4	124
NiAl3.0:1-A	3.0	3.1	0.3037	2.2785	182.2	83
NiAl3.5:1-A	3.5	3.5	0.3036	2.3359	186.5	121
NiAl2.5:1-H	2.5	2.6	0.3027	2.2878	181.5	89
NiAl3.0:1-H	3.0	3.1	0.3047	2.3014	185.0	79
NiAl3.5:1-H	3.5	3.5	0.3049	2.3241	187.1	92

indicated by their composition followed by method of preparation, for example, NiAl2.0:1-A or H indicates the Ni/Al atomic ratio is 2.0 prepared under ageing (A) or hydrothermal (H) treatments, respectively.

3. Results and discussion

Table I shows the calculated and measured compositions of the samples synthesized. It is very clear from this table that there is no marked difference between the two compositions, indicating the completion of precipitation. All the compounds are green in colour owing to the presence of nickel.

XRD of the samples (Fig. 1) indicated the formation of HT-like single phase in the composition range 0.20–0.33, and exhibited sharp and symmetric reflections for (0 0 3), (0 0 6), (1 1 0) and (1 1 3) planes and broad and asymmetric reflections for (1 0 2), (1 0 5) and (1 0 8) planes characteristic of HT-like materials (Hydrotalcite JCPDS 22-700, and Takovite JCPDS 15-87). Samples with a composition outside this range were poorly crystallized or amorphous in nature. However, there is a difference in the intensity of the reflection (see (0 0 6) plane) on going from one sample to another, indicating the different degree of crystallinity, wherein NiAl2.5:1-HT showed the maximum and NiAl3.5:1-A showed the minimum. Furthermore, for NiAl3.5:1-A, the intensity of the higher angle reflections was very low with poor resolution, which was probably due to the presence of amorphous $Ni(OH)_2$ associated with it. These hydrotalcites have rhombohedral 3Rm symmetry with a and c lattice parameters, where c corresponds to three times the thickness of one unit layer. The lattice parameters are calculated by indexing the peaks under a hexagonal crystal system using least-square fitting of the peaks. The lattice parameters and surface area of the samples are also given in Table I. Both the lattice parameters increased with increase in Ni/Al atomic ratio. The increase in the lattice parameter a can be attributed to the higher octahedral ionic radius of Ni^{2+} (0.069 nm) whereas the increase in c can be accounted for on the basis of electrostatic interaction. In other words, with increasing Ni/Al atomic ratio, the extent of interaction between the layer and interlayer decreases, with effective increase in the interlayer spacing. Fig. 2 shows a plot of lattice parameter a with composition, x. A linear relation is observed upto an Ni/Al atomic ratio of 3.0, indicating the operation of Vegard's law. However, at higher concentration (for NiAl3.5:1-A),

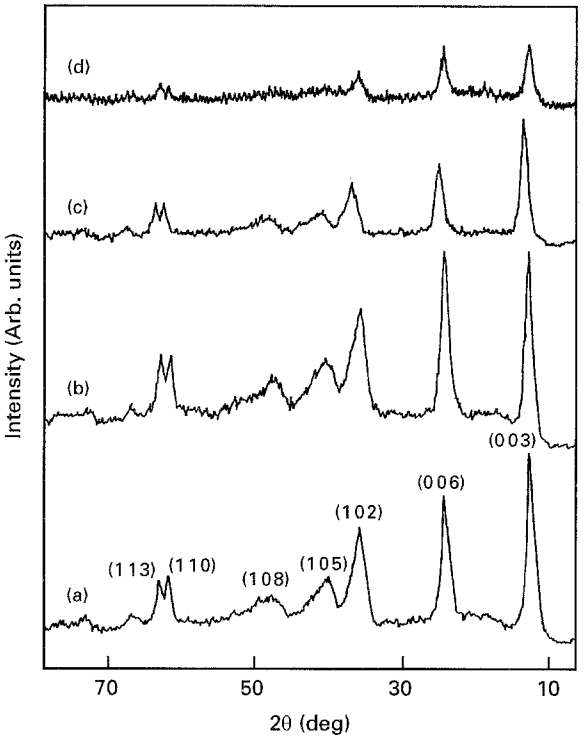

Figure 1 XRD patterns of (a) NiAl2.0:1-A, (b) NiAl2.5:1-A, (c) NiAl3.0:1-A, and (d) NiAl3.5:1-A.

a deviation is observed which could suggest the presence of an amorphous species (because no discrete phase is observed in XRD) along with HT-like phase. We presume this phase to be $Ni(OH)_2$ owing to the excess concentration of nickel ($\sim$ 78 at %). Such a deviation is also observed for Mg–Al HT-like compounds at higher values of Mg/Al atomic ratio [10]. However, the point of occurrence of such a deviation is different for different systems depending on the solubility limit of the bivalent cation in the lattice.

Hydrothermal treatments were performed on aged samples in an attempt to study the changes in the textural properties. As expected, upon this treatment the crystallinity of the material was enhanced as evinced from the increase in the intensity and the sharpness of the peaks in XRD, given in Fig. 3 (see the (0 0 6) plane). This could be due to the agglomeration of small particles to form bigger particles which lead to increased crystallinity. The particle-size measurements were carried out to verify this, using X-ray line broadening [4] and are given in Table II. It is clear from this table that the particle size increased upon hydrothermal treatment. However, the extent of such

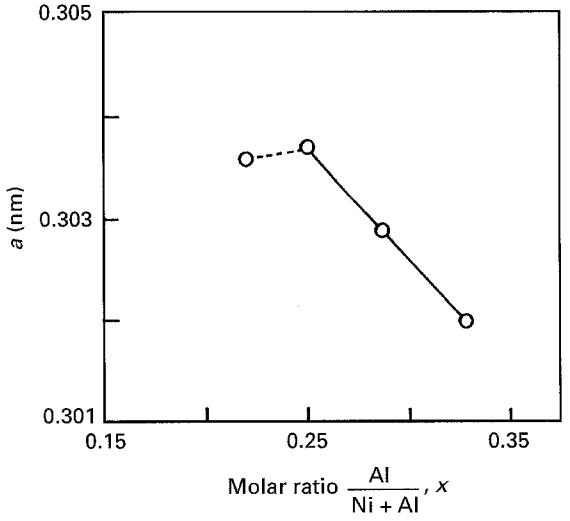

Figure 2 The relation between the ratio Al/Ni + Al and lattice parameter *a*.

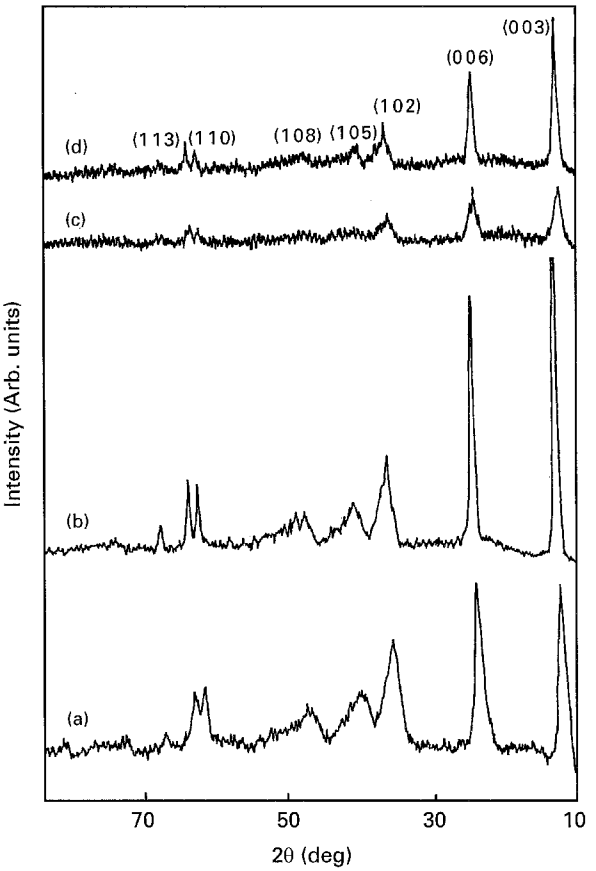

Figure 3 XRD patterns of (a) NiAl2.5:1-A, (b) NiAl2.5:1-H, (c) NiAl3.5:1-A, and (d) NiAl3.5:1-H.

an increase depends on the Ni/Al atomic ratio. The lattice parameters of hydrothermally treated samples given in Table I, indicated that these values were comparable with aged samples. However, a small difference in the cell parameters was observed, especially for NiAl3.0:1-A which could be due to rearrangements associated with a brucite-like layer and an interlayer. Similar to aged samples, an increase in the lattice parameters was observed for hydrothermally treated samples with increasing Ni/Al atomic ratio.

Transmission electron microscopy of these samples showed spherical to hexagonal platelets of thin and wide nature, characteristic of these clay minerals possessing layered structure. However, for these materials, unlike for cobalt and magnesium-containing samples [4], even after extensive dispersion, agglomeration of the particles was observed. This could be due to the inherent property of these samples, which has a tendency for particle–particle interaction.

FT–IR spectra of all the aged samples are given in Fig. 4. They showed absorption bands around 3450 cm^{-1} attributed to hydroxyl stretching, around 1640 cm^{-1} due to the deformation mode of OH, and around 1370 cm^{-1} due to ν_3 carbonate stretching. The low value of ν_{OH} in comparison with the free hydroxyl group (> 3650 cm^{-1}) indicates that all OH groups are hydrogen bonded. However, the extent of such hydrogen bonding depends on the elemental composition. The ν_{OH} band position was shifted to higher wave numbers with an increase in the Ni/Al atomic ratio. This can be explained on the basis of the extent of electrostatic interaction present between the layer and the interlayer with a consequent effect on hydrogen bonding. A weak absorption band around 2950 cm^{-1} is observed which is attributed to water molecules hydrogen bonded to carbonate ions in the interlayer. ν_2 (out-of-plane deformation) and ν_4 (in-plane bending) of carbonate were observed around 880 and 665 cm^{-1}, respectively. The differences noticed for all bands between observed vibrations of carbonate and free carbonate indicates even perturbation of the anion in the interlayer space. A few bands were also observed around 1700, 1230, 1160 and 1110 cm^{-1} for these samples, indicating the presence of nitrate [11]. The source of the nitrate ion could be from the precursor metal nitrates. We have observed for the first time, the presence of nitrate ions along with carbonate as the charge-balancing anion in the interlamellar space of Ni–Al hydrotalcites. The other

TABLE II Particle sizes of aged and hydrothermally treated samples by X-ray line broadening

Compound	2θ (deg)	*hkl*	β (rad)	*t* (nm)	Av. *t* (nm)
NiAl2.5:1-A	23.760	006	0.021	6.7	7.9
	61.260	110	0.017	9.1	
NiAl2.5:1-H	23.088	006	0.010	16.0	20.9
	61.260	110	0.007	25.7	
NiAl3.5:1-A	23.246	006	0.021	6.7	9.0
	59.870	110	0.014	11.3	
NiAl3.5:1-H	22.872	006	0.014	12.0	13.6
	60.820	110	0.010	15.2	

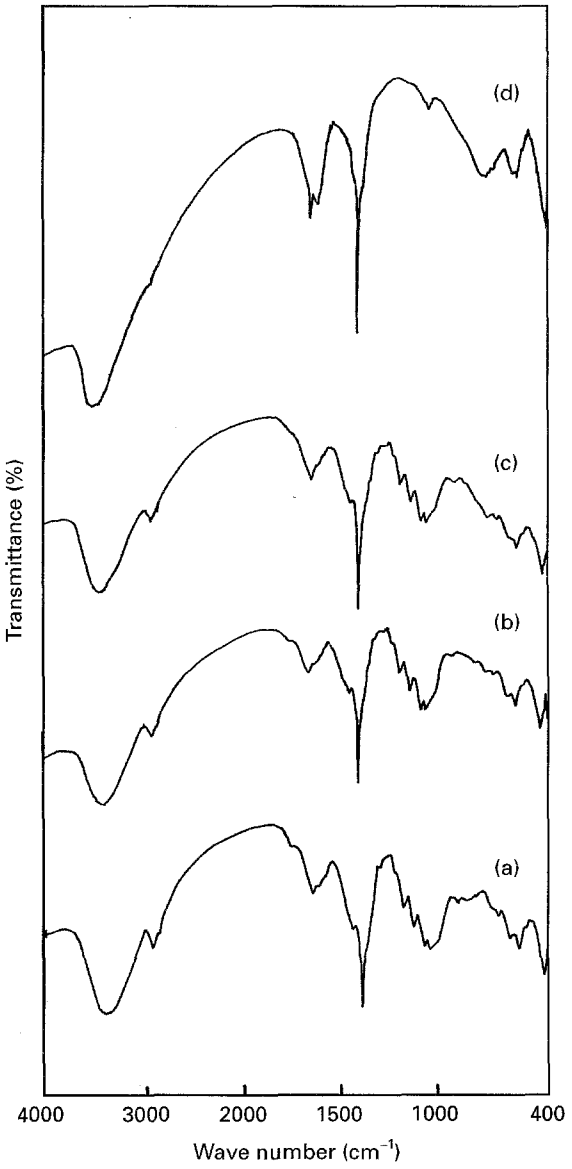

Figure 4 FT–IR spectra of aged samples: (a) NiAl2.0:1-A, (b) NiAl2.5:1-A, (c)NiAl3.0:1-A, and (d) NiAl3.5:1-A.

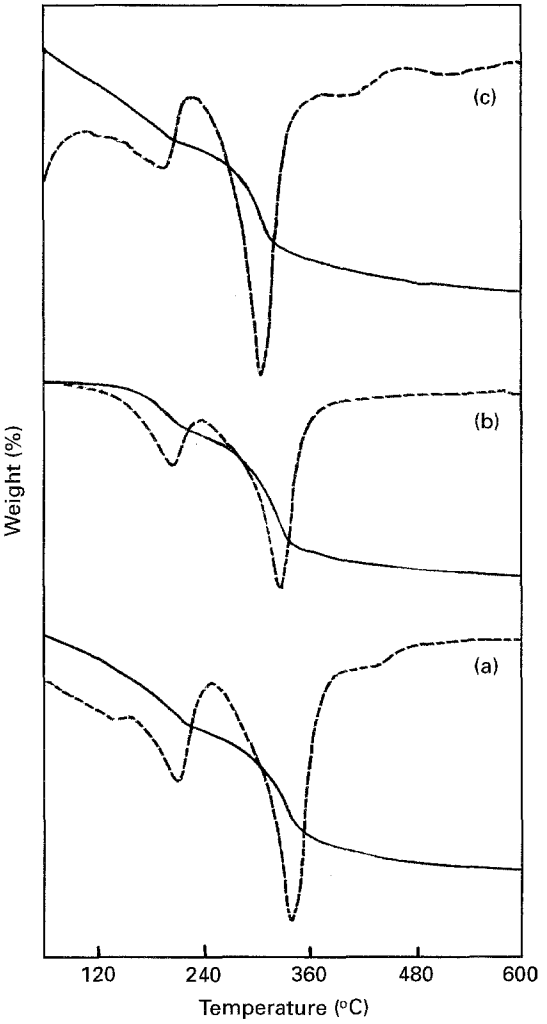

Figure 5 TG–DTG traces of aged samples: (a) NiAl2.0:1-A, (b) NiAl2.5:1-A, and (c) NiAl3.0:1-A. (—) TG, (– – –) DTG.

bands observed in the region 800–400 cm^{-1} (600, 560 and 425 cm^{-1}) are assigned for lattice vibrations like Ni–O–Al bending and Ni(Al)–O stretching.

In all the samples, the ν_3 mode of carbonate exhibited a sharp band around 1380 cm^{-1} with a shoulder around 1430 cm^{-1}. This could be due to lower symmetry of the carbonate present in the interlayer. For a symmetrical carbonate to be present in the interlayer, it should be present parallel to the interlayer sheet with D_{3h} symmetry. Owing to its interaction with OH species present in the brucite-like sheet and water molecules in the interlayer, the symmetry becomes reduced to C_{3v} or C_{2v} which causes splitting in the ν_3 mode. Such a split is also noticed for the ν_4 band of carbonate observed around 690 cm^{-1}. This can also cause activation in the ν_1 mode observed around 1020 cm^{-1}, which is IR forbidden when the carbonate is present in a symmetric environment. Hydrothermal treatment was performed in an attempt to enhance the orderliness in the interlayer sheet. However, such a split in the ν_3 band with the ν_1 band was observed even after this treatment, indicating the poor ordering of the anion in the interlamellar space. Furthermore, there is no significant shift in the band position of ν_{OH} and ν_3 of the carbonate upon hydrothermal treatment, which is in contrast to the results reported by Labajos *et al.* [12] for Mg–Al hydrotalcite.

Fig. 5 shows the TG–DTG pattern of all the aged samples prepared. All the compounds, similar to natural mineral takovite [13], showed two stages of weight loss. The first weight loss occurred around 200 °C and was attributed to the removal of physisorbed and interlayer water molecules. The second weight loss, observed around 310 °C, was associated with removal of water from the brucite-like sheets and CO_2 from the interlayer carbonate anion (also gases like NO, NO_2 from the nitrate) with the destruction of the layered structure. The corresponding peak appeared broad because two processes, namely dehydroxylation and decarbonation, take place simultaneously. Furthermore, a small continuous weight loss was observed up to 600 °C which can be hypothesized to be the complete elimination of carbonate anions. The TG peak temperatures and net weight loss of the samples are given in Table III. It can be inferred from the table that both temperatures T_1 and T_2 increased with the decrease in Ni/Al atomic ratio. Substitution of Ni^{2+} by Al^{3+} increases the positive charge density of the

TABLE III TG–DSC peak temperature for aged and hydrothermally treated samples

Compound	TG temp. (°C)		Net weight loss (%)	DSC temp. (°C)	
	T_1	T_2		T_1	T_2
NiAl2.0:1-A	198	313	36.7	265	377
NiAl2.5:1-A	204	325	29.2	230	356
NiAl3.0:1-A	191	303	35.6	219	336
NiAl3.5:1-A	203	300	36.0	227	344
NiAl2.5:1-H	248	366	32.8	253	355
NiAl3.0:1-H	213	350	32.7	235	336
NiAl3.5:1-H	234	349	34.6	250	358

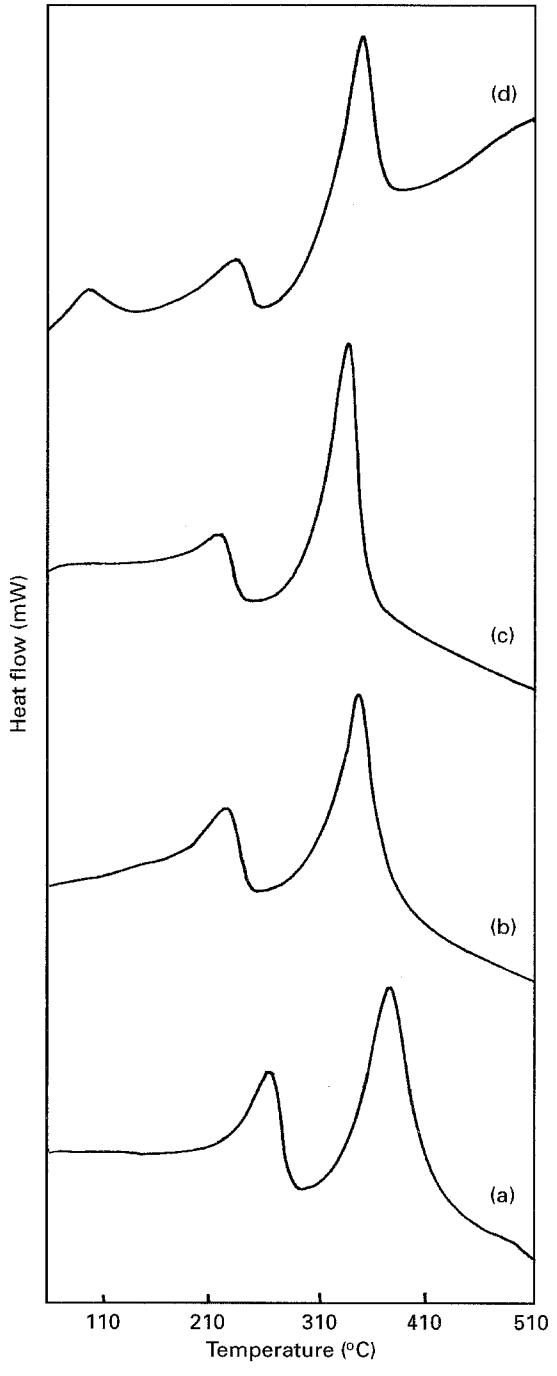

Figure 6 DSC traces of (a) NiAl2.0:1-A, (b) NiAl2.5:1-A, (c) NiAl3.0:1-A, and (d) NiAl3.5:1-A.

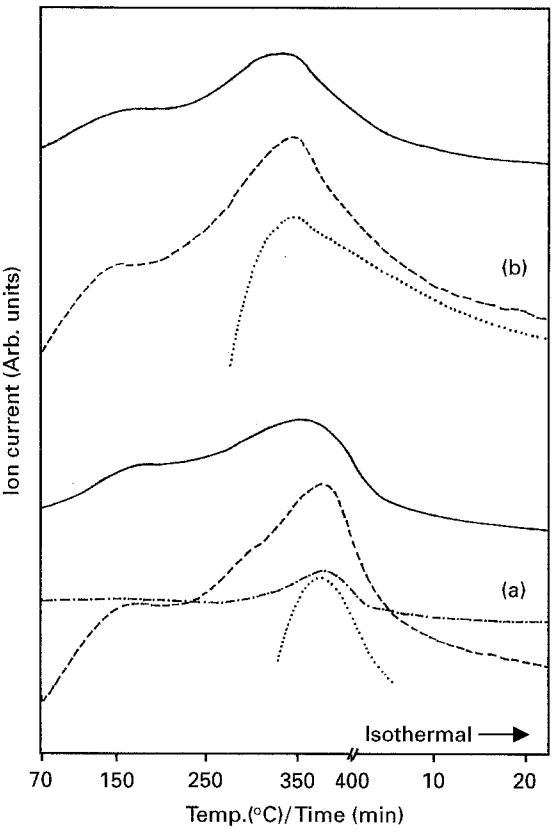

Figure 7 EGA patterns of (a) NiAl3.0:1-A, and (b) NiAl3.5:1-A. (—) H_2O, (– – –) CO_2, (—·—) N_2, (···) NO.

layer which increases the electrostatic interaction between the layer and the interlayer, thereby causing the shift in the temperature to the higher side.

The DSC results (Fig. 6) substantiated the TG results showing two endotherms for the corresponding two weight losses. No additional peaks were found in the DSC of hydrothermally treated samples (figure not given) indicating that no new phases are formed upon this treatment and only HT-like phase is present. Comparison of DSC curves of aged and hydrothermally treated samples showed that the curves are sharper and more intense for the latter, indicative of their higher crystallinity (cf. XRD results). The DSC peak temperatures are also given in Table III. Although there is a considerable difference between TG and DSC temperatures (which could be due to different flow rates of the carrier gas employed during TG–DSC measurements), the DSC peak temperatures increased with decreasing Ni/Al atomic ratio, substantiating TG results.

In order to obtain a better understanding of thermal decomposition sequence, evolved gas analysis (EGA) has been carried out using a quadruple mass spectrometer (Balzers GAM 440). The samples were heated from room temperature to 400 °C with 10 °C/cycle (or 10 °C min^{-1}) and the evolved gases whose mass numbers in the range 1–60 were analysed. Fig. 7 show the EGA patterns of some of the samples prepared. Two stages of weight loss corresponding to water were observed at a temperature around 150 and 380 °C. However, for CO_2 ($m/e = 44$) an initial loss was observed around 150 °C (below the first transformation temperature, T_1). This could be due to the

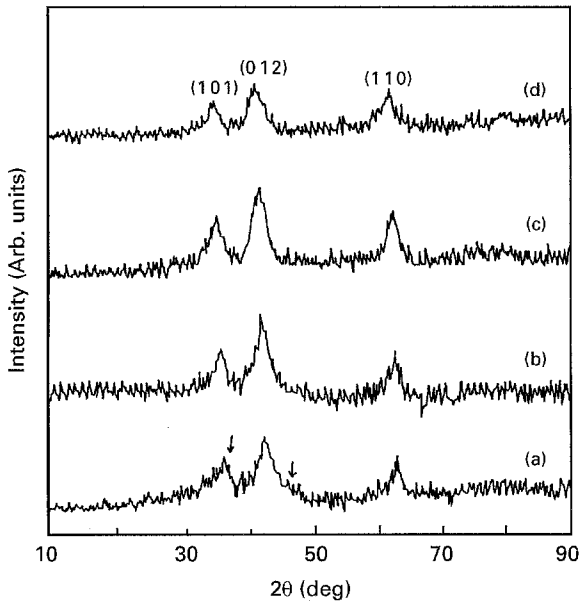

Figure 8 XRD patterns of (a) NiAl2.0:1-A, (b) NiAl2.5:1-A, (c) NiAl3.0:1-A, and (d) NiAl3.5:1-A calcinated at 450 °C for 5 h in air.

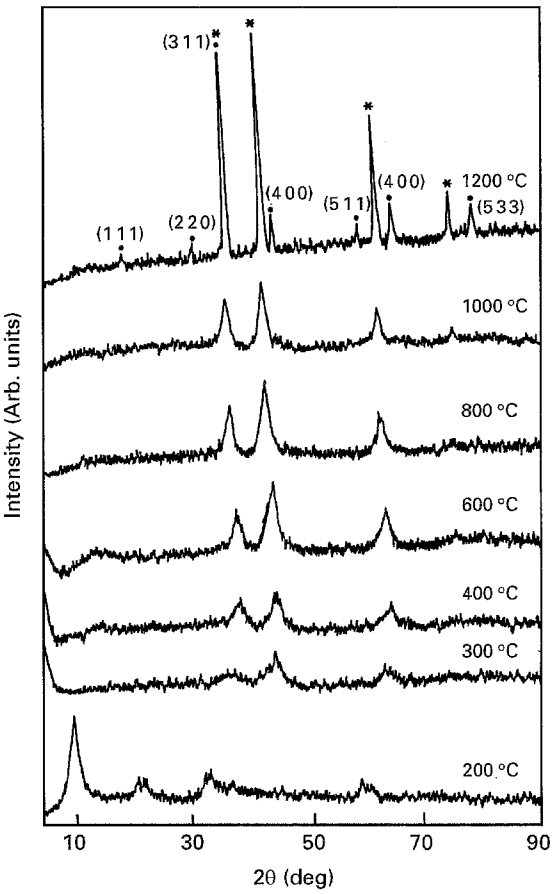

Figure 9 XRD pattern of NiAl3.0:1-A calcined at various temperatures for 1 h. (*) NiO, (●) spinel.

removal of the carbonate anion present at the edges of the interlayer where the interaction exerted between the layer and the interlayer is minimum. The CO_2 loss corresponding to a second stage of transformation occurs in two stages (around 250–300 and 380 °C). This could imply the presence of two different types of carbonate. At present it is very difficult to ascertain the two types of carbonate species. One could possibly perceive that the two types of carbonate are first that closer to the brucite-like sheet and second that in the interior of the interlayer. This could also be due to the difference in the interaction of the carbonate ion with Ni^{2+} and Al^{3+} in the lattice. To our knowledge, we have observed for the first time the presence of three different types of carbonate in the interlayer space. Furthermore, gases with mass numbers 28, 30 and 46 were also observed for these samples and correspondingly attributed to N_2, NO and NO_2, confirming the presence of nitrate in the interlayer space (cf. FT–IR).

Fig. 8 show the XRD pattern of aged samples calcined at 450 °C for 5 h in air. All the samples showed a poorly crystalline NiO. However, the crystallinity of NiO was affected with composition. Better crystalline material was obtained for the sample with a lower aluminium content (cf. Fig. 8a and c). The XRD of the calcined NiAl2.0:1-A sample showed weak diffraction lines (arrowed) corresponding to γ-Al_2O_3 and/or a spinel-type phase apart from NiO. This could be due to the higher aluminium content of this sample. Table IV give the phase obtained, particle size, lattice parameters and surface area of the calcined samples. The particle size was calculated by the line-broadening method using the (0 1 2) plane after correcting for instrumental broadening. The size was unaffected with respect to composition except for the sample NiAl2.0:1-A, which showed the smallest size (3.6 nm). The lattice parameter values calculated for these oxides are lower than those for pure NiO which indicate the dissolution of Al^{3+} (0.053 nm) in the NiO lattice, forming a solid solution $NiAl_{2\delta}O_{1+3\delta}$.

Fig. 9 indicates the variation in the XRD pattern of the sample NiAl3.0:1-HT with calcination temperature. The sample was kept at each temperature for 1 h under an air atmosphere. The sample was stable up to 200 °C exhibiting diffraction lines corresponding to HT-like structure. However, a reduction in the intensity of the peaks with concomitant shift in the (0 0 3) reflection to higher angle was observed. This

TABLE IV Phase obtained, particle size, lattice parameters and surface area of the aged samples calcined at 450 °C for 5 h in air

Compound	Phase obtained	Particle size (nm)	a (nm)	c (nm)	V (10^{-3} nm^3)	Surface area ($m^2 g^{-1}$)
NiAl2.0:1-A	NiO	36	0.2947	0.7260	54.6	170
NiAl2.5:1-A	NiO	53	0.2934	0.7200	53.7	146
NiAl3.0:1-A	NiO	47	0.2935	0.7211	53.8	137
NiAl3.5:1-A	NiO	45	0.2950	0.7125	53.7	92
NiO[a]	–	–	0.2954	0.7236	54.7	–

[a] JCPDS 22–1183.

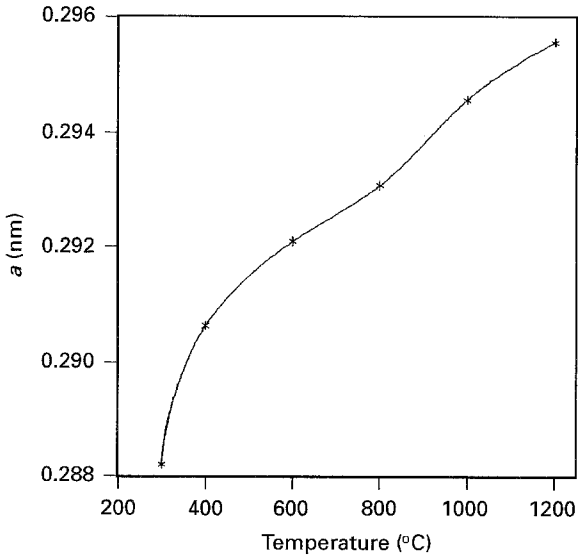

Figure 10 Variation of NiO lattice parameter a with calcination temperature for NiAl3.0:1-A.

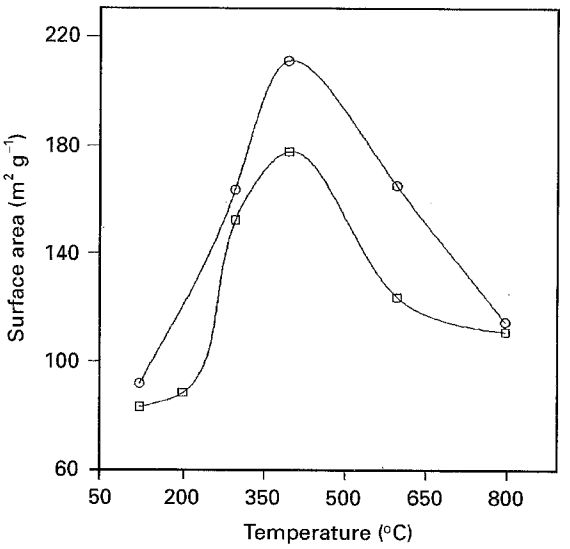

Figure 11 Variation of surface area with calcination temperature. (○) NiAl2.0:1-HT, (□) NiAl3.0:1-HT.

could be due to the removal of interlayer water molecules, thereby affecting the interlayer thickness. Calcination above this temperature (> 300 °C) resulted in poorly crystalline NiO. Although mixed metal oxides obtained in the temperature range 400–800 °C are poorly crystallized, they are characterized by unusual properties, such as high thermal stability, good dispersion, high surface area and low reducibility. From recent studies [14], a decoration model has been proposed for the thermally calcined Ni–Al hydrotalcites consisting of three phases, namely (1) an NiO phase, probably containing Al^{3+} impurities; (2) a spinel-type phase, located on the surface of NiO; and (3) a nickel-doped Al_2O_3 phase possibly grafted on NiO and/or spinel phase. In other words, the NiO crystallites can be viewed as oxide decorated by spinel-type phase. Such decoration would decrease the oxide sintering through interparticle bridging. The crystallinity of the oxide increased with increasing calcination temperature (up to 900 °C) as evinced by the increase in intensity and sharpness of the peaks (see the (0 1 2) peak). The lattice parameters calculated for these oxides also shifted towards pure NiO, indicating the decrease in lattice distortion. Fig. 10 shows the variation in the lattice parameter with calcination temperature. On further increase in the temperature of calcination (> 1000 °C) phase separation to NiO and $NiAl_2O_4$ was observed. The demixing of the metal oxides was more pronounced for the sample calcined at 1200 °C.

The observed X-ray results can be substantiated by surface-area measurements. Fig. 11 shows the variation of surface area with calcination temperature for some of the samples, the sample being calcined for 1 h at each temperature. They showed an initial increase in the surface area up to 300 °C. This could be due to the formation of micropores due to the expulsion of H_2O and CO_2 from the sample. Further increase in the temperature resulted in the loss of surface area, which could be attributed to the sintering of metal oxide particles. However, the extent of the initial increase, as well as the contraction in surface area, depends on the Ni/Al atomic composition. The sample with higher aluminium content showed higher initial increase and slow drop rate in the surface area. This is because, the formation of aluminium-containing compounds would be more facile for the sample with higher aluminium content, which would, in turn, prevent interparticle interaction among NiO through decoration and dispersion. Such an effect would increase the thermal stability of NiO particles by preventing them from sintering. However, at higher calcination temperatures (> 800 °C), phase separation occurs and hence the surface-area values are not affected significantly with composition.

4. Conclusions

1. All the compounds synthesized in the composition range (x = 0.20–0.33) were single phase with HT-like structure.
2. The lattice parameters (a and c) increased and the thermal stability decreased for these samples with increasing Ni/Al atomic composition.
3. IR and EGA studies confirmed the presence of nitrate along with carbonate, as the charge-balancing anion in the interlayer of these compounds.
4. EGA studies showed the presence of three different types of carbonate present in the interlayer.
5. Thermal calcination of these materials yielded NiO whose crystallinity and thermal stability were affected both by composition and calcination temperature.

Acknowledgements

The research work was supported by a grant from Air Products Chemicals Inc. which we gratefully acknowledge. The authors thank Mr Suresh Sriram in the preliminary studies and Mrs Kanchanamala, Department of Metallurgy, for assistance in TEM studies.

References

1. F. CAVANI, F. TRIFIRO and A. VACCARI, *Catal. Today* **11** (1991) 173.
2. W. REICHLE, *CHEMTECH* **16** (1986) 58.
3. C. S. SWAMY, S. KANNAN and S. VELU, in "2nd ANAIC International Conference on Material Science and Environmental Chemistry of Main Group Elements", Kaula Lumpur, Malaysia, 8–11 November (1993) in press.
4. S. KANNAN and C. S. SWAMY, *J. Mater. Sci. Lett.* **11** (1992) 1585.
5. *Idem, Appl. Catal. B* **3** (1994) 109.
6. S. KANNAN, S. VELU, V. RAMKUMAR and C. S. SWAMY, *J. Mater. Sci.* **30** (1995) 1462.
7. S. VELU and C. S. SWAMY, *Appl. Catal.* **119** (1994) 241.
8. O. CLAUSE, B. REBOURS, E. MERLEN, F. TRIFIRO and A. VACCARI, *J. Catal.* **133** (1992) 231.
9. S. KANNAN and C. S. SWAMY, "Preparation of catalysts VI", in "Studies in Surface Science and Catalysis (Vol. 91), edited by G. Poncelet, J. Martens, B. Delmon, P. A. Jacobs and P. Grange (Elsevier, Amsterdam, 1995) p. 903.
10. H. SCHAPER, J. J. BERG-SLOT and W. H. J. STORK, *Appl. Catal.* **54** (1989) 79.
11. S. MIYATA, *Clays Clay Miner.* **23** (1975) 369.
12. F. M. LABAJOS, V. RIVES and M. A. ULIBARRI, *J. Mater. Sci.* **27** (1992) 1546.
13. D. L. BISH and G. W. BRINDLEY, *Am. Mineral.* **62** (1977) 458.
14. B. REBOURS, J-B D'ESPINOSE DE LA CAILLERIE and O. CLAUSE, *J. Am. Chem. Soc.* **116** (1994) 1707.

Received 2 May
and accepted 20 November 1995